HHS Public Access

Author manuscript

Nat Methods. Author manuscript; available in PMC 2018 April 09.

Published in final edited form as:

Nat Methods. 2017 November ; 14(11): 1075–1078. doi:10.1038/nmeth.4461.

Achieving better than 3 Å resolution by single particle cryo-EM at 200 keV

Mark A. Herzik Jr.[*], **Mengyu Wu**[*], and **Gabriel C. Lander**

Department of Integrative Structural and Computational Biology, The Scripps Research Institute, La Jolla, California 92037, USA

Abstract

Nearly 98% of single particle cryo-EM structures resolved to better than 4 Å resolution have been determined using 300 keV transmission electron microscopes. We demonstrate that it is possible to obtain reconstructions of macromolecular complexes at a range of sizes to better than 3 Å resolution using a 200 keV transmission electron microscope. These structures are of sufficient quality to unambiguously assign amino acid rotameric conformations and identify ordered water molecules.

Introduction

Recent technical breakthroughs in the field of three-dimensional single-particle cryo-electron microscopy (cryo-EM) have allowed for the visualization of biological macromolecular assemblies in near-native states at unprecedented resolutions[1, 2]. To date, the vast majority of high-resolution cryo-EM reconstructions have been obtained using transmission electron microscopes (TEMs) operating at 300 keV equipped with a direct electron detector (DED). TEMs operating at 300 keV offer minimized inelastic scattering and specimen charging over those at lower voltages, the benefits of which confer an advantage in imaging thicker specimens[3]. However, the high cost of purchasing and operating high-end TEMs may be unfeasible for many institutions. Here we expand upon prior studies utilizing 200 keV TEMs[4,5], and demonstrate that a Thermo Fisher Talos Arctica (200 keV) paired with a Gatan K2 Summit can produce cryo-EM reconstructions of *Thermoplasma acidophilum* 20S proteasome and rabbit muscle aldolase at ~3.1 Å and ~2.6 Å resolution, respectively. The resulting maps are of sufficient quality to identify ordered

Correspondence to: Gabriel C. Lander (glander@scripps.edu).

[*]authors contributed equally to this work

Author contributions

M.A.H and M.W performed all cryo-EM experiments and analyses. All authors contributed to the experimental design and manuscript preparation.

Competing financial interests

The authors declare no competing financial interests.

Data availability. The coordinates for the 20S stage position, 20S image shift, and aldolase structures are deposited in the Protein Data Bank with the PDB IDs 5VY3, 5VY4, and 5VY5, respectively. The corresponding EM density maps have been deposited to the Electron Microscopy Data Bank with the EMDB IDs 8741, 8742, and 8743, respectively. The datasets that support the findings of this study are also available from the corresponding author upon request.

water molecules and unambiguously assign amino acid rotameric conformations. Our work represents a significant advancement in the attainable resolution limit for structures obtained using a 200 keV TEM, proving that such TEMs equipped with a DED are capable of reconstructing macromolecules of varying sizes and symmetries at resolutions previously ascribed only to 300 keV microscopes.

Results

Data Collection and Processing Strategy

All data were acquired using a base-model Talos Arctica TEM operating at 200 keV. Careful alignment of the TEM was performed before each data collection to maximize parallel illumination[6] (see **Methods** and **Protocol Exchange DOI**) (Supplementary Figure 1) and ensure Thon rings were visible beyond ~3 Å resolution in the power spectrum of images collected over amorphous carbon. Coma-free alignment was performed according to Glaeser *et al.*[6] immediately prior to data collection, as implemented in Leginon[7]. Data were collected using Leginon[7] and image pre-processing was performed using the Appion pipeline[8]. Images were acquired at a nominal magnification of 45,000× (calibrated pixel size of 0.91 Å at detector level) with the Gatan K2 Summit DED operating in super-resolution mode. To minimize the effects of electron beam-induced motions, samples were prepared on gold grids[9] and exposures were acquired at the center of holes (1.2 μm diameter) using a beam (~2 μm diameter) large enough to cover the entirety of the hole and contact the surrounding gold substrate.

Mechanical and beam-induced motions were corrected and dose weighting performed using MotionCor2[10]. Whole-image contrast transfer function (CTF) estimation was performed using CTFFind4[11] and micrographs yielding CTF estimates below an Appion confidence value of 0.9 were discarded. Per-particle CTF estimates calculated using gCTF[12] were utilized for all subsequent processing steps. Reference-free 2D classification and subsequent 3D classification and 3D auto-refinement were performed using RELION 2.0[13]. All reported resolutions are based on the gold-standard Fourier shell correlation (FSC) criterion[14] (see **Methods**).

Structures of the 20S proteasome at ~3.1 Å and ~3.3 Å resolution

To assess the resolving capabilities of a Talos Arctica TEM we sought to determine the structure of the *Thermoplasma acidophilum* 20S proteasome, a symmetric ~700 kDa protein complex with high thermal stability, previously determined to ~2.8 Å resolution using cryo-EM[15]. We collected 629 movies of frozen-hydrated 20S (Figure 1) with a defocus range of −0.8 μm to −1.8 μm using stage movements to navigate to each desired exposure target. A final stack of 106,581 particles yielded a reconstruction estimated as ~3.1 Å resolution (Figure 1 and Supplementary Figure 2, see **Methods**). Local resolution estimation of this EM density indicates that most of the map resolved to better than ~3.2 Å resolution, with the core of the molecule resolved to ~2.8 Å resolution (Figure 1 and Supplementary Figure 2). Indeed, an overlay of the ~2.8 Å 20S proteasome reconstruction EMD-6287 reveals that the EM densities are of comparable quality, with both maps possessing clearly resolvable side-chain densities (Supplementary Figure 3).

As an alternative data collection strategy to using stage position navigation, images were collected using stage position to navigate to the center of 4 holes before image shifting the beam to each exposure target (Supplementary Figure 4). This data collection strategy has the benefit of being able to collect more micrographs per hour, on average (Supplementary Table 1). However, substantial image shifting can introduce coma, which manifests as phase error in the structure factors. To determine the extent to which beam tilting affects the attainable resolution, we collected 394 movies of frozen-hydrated 20S using image shift to navigate to acquisition targets. Using a similar data processing and refinement strategy as employed for the stage position dataset, a final stack of 96,254 particles yielded a ~3.3 Å resolution reconstruction (Figure 1 and Supplementary Figure 5). An estimation of the local resolution of this EM density indicates that most of the map resolves to ~3.2 Å resolution or better, with parts of the core resolved to better than 3 Å (Figure 1).

Comparison of the two 20S reconstructions generated using our 200 keV TEM reveals that maps of comparable quality can be obtained with less than ~0.2 Å resolution loss when using image shift versus stage position for exposure target navigation. Visual inspection of the 20S EM densities indicates only modest differences in side-chain resolvability (Figure 1), suggesting that the extent of the coma introduced through our image shift navigation strategy minimally disrupts optimal image formation (see Supplementary Note 1).

The best-resolved regions of the 20S reconstruction from the stage movement dataset features density that can be attributed to well-ordered water molecules (Figure 1). Importantly, the location of many of these waters correlate with those previously observed for the *T. acidophilum* 20S proteasome determined by cryo-EM (EMD-6287) and X-ray crystallography (PDB ID: 1YAR) (Supplementary Figure 3). Further examination of the density reveals that some side chains exhibit alternative conformations that lie within expected rotameric positions (Figure 1). To the best of our knowledge, these are the first observations of water molecules and/or alternative side-chain conformations in a reconstruction obtained using a 200 keV TEM.

Structure of rabbit muscle aldolase at ~2.6 Å resolution

All structures except one (EMD-6337) determined to better than 5 Å resolution using a 200 keV TEM possess high internal symmetry (EMDs-2791; 5886) and/or comprise a molecular weight of ≥700 kDa (EMDs-5247; 5592; 6458). In fact, only 2 structures less than 200 kDa have been reported to better than 3 Å resolution (EMDs-8191 and 3488), both determined using a 300 keV TEM. To determine whether near-atomic resolution was feasible for complexes in this size range using a 200 keV TEM, we sought to determine the structure of aldolase, a ~150 kDa homotetrameric enzyme (see **Methods**).

784 movies of frozen-hydrated aldolase (Supplementary Figure 6) were collected using similar acquisition settings as those used for the 20S proteasome. A final stack of 83,910 particles yielded a ~2.6 Å resolution reconstruction (see **Methods,** Figure 2, and Supplementary Figure 6). Local resolution estimates reveals that most of the map is resolved to better than 2.8 Å with the best-ordered regions of the map resolved to ~2.5 Å (Figure 2). The final reconstruction possesses clear side-chain density for most of the molecule and well-resolved backbone density. The best-refined model agrees well with previously

published structures determined by X-ray diffraction methods, with an overall RMSD of 0.45 Å (PDB ID: 6ALD). Further examination of the density reveals that the best resolved regions of the map possess densities attributed to ordered water molecules (Figure 2). Moreover, the positions of these water molecules are conserved between those identified in PDB ID: 6ALD (Supplementary Figure 7).

Discussion

TEMs operating at 300 keV have been shown to be optimal for imaging thicker biological specimens due to reduced inelastic scattering, which limits image blurring associated with charging effects and radiolysis[3, 16]. The deleterious effects of beam-induced motion and radiation damage can be accounted for computationally through fractionation into movie frames using a DED[10, 17–21]. For these reasons, 300 keV TEMs coupled with DEDs remain the flagship instruments in the field of high-resolution single-particle cryo-EM, accounting for nearly 98% of all reconstructions reported to 4 Å resolution or better. The results presented in this study demonstrate that cryo-EM reconstructions resolved to ~3 Å resolution and better are achievable using a 200 keV TEM coupled with a K2 Summit DED for samples of different sizes and internal symmetries. The maps generated herein are of sufficient quality for *de novo* model building as well as identification of ordered waters and alternative side-chain conformations (Figures 1 and 2).

Several studies have used *T. acidophilum* 20S proteasome as a metric for characterizing the potential of TEMs and imaging accessories[2, 4, 15, 18]. We similarly sought to assess the resolution limit of the Talos Arctica using the 20S. Notably, both 20S reconstructions exhibited clear density attributed to ordered water molecules, an unprecedented achievement for structures obtained using a 200 keV TEM. The presence of alternative amino acid rotamers in the density map further attests to the quality of the reconstruction.

To contrast the 20S proteasome, which benefits from size, high internal symmetry, and high thermostability, and to assess the resolving capacity of a 200 keV TEM for smaller complexes, we also imaged rabbit muscle aldolase. Using similar illumination conditions as those utilized for determining the structures of 20S proteasome, the final aldolase reconstruction achieved a resolution of ~2.6 Å. While the smaller size of aldolase and thus the fewer voxels utilized in the calculation of FSC may partly influence the higher reported resolution for aldolase relative to the 20S, it is also likely that the smaller size of aldolase contributes to a more isotropic resolution that is not negatively influenced by flexible peripheral domains. However, differences in ice thickness, overall sample stability, and minor differences in microscope alignment cannot be ruled out as contributors.

Typically, micrometer underfocus values have been prescribed for imaging targets less than 200 kDa[22]. More recently, strategies implementing phase plates combined with a small amount of defocus to boost image contrast have been demonstrated to be an effective method for resolving small protein complexes[23]. However, despite the small size of the aldolase particles used in this study, micrographs of sufficient contrast were obtained using underfocus values as low as −0.6 μm (Supplementary Table 1). We believe this is largely attributed to the thin ice of the aldolase specimen, coupled with high particle density to boost

particle contrast in the collected micrographs and facilitate alignment of movie frames. Our results suggest it is feasible to achieve near-atomic resolution reconstructions of a sub-200 kDa specimen using a conventional defocus approach (see Supplementary Note 2).

We regard this work as a demonstration of the capabilities of a 200 keV TEM, rather than a comparison of the benefits of operating at either 200 or 300 keV. Performing such a comparison would require great care in ensuring consistency in as many parameters as possible, including specimen quality, imaging conditions (e.g. magnification, defocus range, pixel size, etc.), and data processing. Ideally, such experiments would be performed on a single grid using a microscope that is capable of operating at either 200 or 300 keV.

The specimens examined herein were selected for their robust structural integrity and limited conformational heterogeneity to probe the resolution capabilities of a 200 keV TEM. We recognize that not all samples are as well behaved as those presented in this study; nonetheless, our findings serve as an important proof-of-principle for near-atomic resolution structure determination on a 200 keV TEM. Given that the cost of the Talos Arctica used in this study is approximately less than half that of a 300 keV Titan Krios, it is our hope that this work expands the field of high-resolution cryo-EM to a broader range of research institutes that are unable to incur the steep long-term financial commitment of a 300 keV TEM.

Online methods

Cryo-electron microscopy sample handling and grid preparation

Pure aldolase isolated from rabbit muscle was purchased as a lyophilized powder (Sigma Aldrich) and solubilized in 20 mM HEPES (pH 7.5), 50 mM NaCl at ~3 mg/ml. Aldolase was further purified by size-exclusion chromatography using a Sepharose 6 10/300 (GE Healthcare) column equilibrated in solubilization buffer. Peak fractions were pooled and concentrated to 1.6 mg/ml immediately prior to cryo-electron microscopy (cryo-EM) grid preparation.

Archaeal 20S proteasome (*T. acidophilum*) was kindly donated by Drs. Zanlin Yu and Yifan Cheng at The University of California, San Francisco and used as-is without further modification.

For cryo-EM, 3 μL of purified aldolase (1.6 mg/ml) or 20S proteasome (0.5 mg/ml) were dispensed on freshly plasma cleaned UltrAuFoil® R1.2/1.3 300-mesh grids (Electron Microscopy Services) and manually blotted[25] using a custom-built manual plunger in a cold room (≥95% relative humidity, 4°C). Sample was blotted for ~4 seconds with Whatman No. 1 filter paper immediately prior to plunge freezing in liquid ethane cooled by liquid nitrogen. In order to provide enough signal for proper CTF estimation we strived to achieve a particle concentration that maximized the number of particles contained within the holes without resulting in overlapping particles and/or aggregation (see Supplemental Note 3).

Cryo-EM data acquisition, image processing, and refinement

Microscope alignments were performed on a cross-grating calibration grid. Condenser alignments and stigmation were performed as described previously for a two condenser lens system[26]. Proper eucentric height of the specimen was determined using Leginon prior to setting focus. Parallel illumination of the beam was maximized in diffraction mode by first adjusting the defocus to bring the objective aperture into focus in the front focal plane of the diffraction lens followed by adjustments of beam intensity to minimize the spread of gold powder diffraction[27] (Supplementary Figure 1). The resulting beam intensity value was saved in Leginon and remained unchanged throughout data collection. The objective aperture was centered and any objective lens astigmatism was minimized. Exposure rate measurements on the K2 Summit DED were then collected to determine whether changes to spot size were necessary to achieve the desired exposure rate. In the event that changes in exposure rate were required, as was the case for increasing per frame cumulative dose during aldolase imaging, adjustments to spot size were made and alignments were repeated, including maximization of parallel illumination. Coma-free alignment was then performed as described previously[6] **(Protocol Exchange DOI)**. Daily adjustments, if necessary, were made during data collection to maintain lens stigmation and ensure the beam was coma-free.

All cryo-EM data were acquired using the Leginon automated data-acquisition program[7]. All image pre-processing (frame alignment, CTF estimation, particle picking) were performed in real-time using the Appion image-processing pipeline[8] during data collection.

Images of frozen hydrated aldolase or 20S proteasome were collected on a Thermo Fisher Talos Arctica transmission electron microscope (TEM) operating at 200 keV. Movies were collected using a Gatan K2 Summit direct electron detector operating in super-resolution mode (super-resolution pixel size 0.455 Å/pixel) at a nominal magnification of 45,000x corresponding to a physical pixel size of 0.91 Å/pixel.

629 movies (68 frames/movie) of 20S proteasome were collected using stage position to navigate to the exposure target. Movies were collected over 17 seconds exposure with an exposure rate of 3.2 e^{-}/pixel/s, resulting in a total exposure of ~65 $e^{-}/Å^2$ (0.96 $e^2/Å^2$/frame) and a nominal defocus range from −0.8 μm to −2.8 μm. The same exposure settings were used to collect 394 movies using image shift target navigation. Super-resolution images were Fourier-binned 2 x 2 (0.91 Å/pixel) prior to motion correction and dose-weighting using the MotionCor2 frame alignment program[10] as part of the Appion pre-processing workflow. Frame alignment was performed on 5 x 5 tiled frames with a B-factor of 100 applied. Unweighted summed images were used for CTF determination using CTFFIND4[11]. DoG picker[28] was used to automatically pick particles from the first 10 dose-weighted micrographs yielding a stack of 4,821 particles that were binned 8 x 8 (3.64 Å/pixel, 92 pixel box size) and subjected to reference-free 2D classification using an iterative topology-representing network-based classification followed by multi-reference alignment[29] in the Appion pipeline. The best 4 classes were then used for template-based particle picking against the each dataset using FindEM[30]. Only micrographs fulfilling the following two criteria: 1) possessing a CTF estimate confidence of fit ≥90% and 2) with resolution

estimates to 5 Å or better at CC=50% (359 total from the stage position data set; 283 total from the image shift data set) were used.

For the 20S proteasome data set collected using stage position, 153,429 particles were extracted rom the dose-weighted summed images, further binned 4 x 4 (3.64 Å/pixel, 92 pixel box size), and subjected to reference-free 2D classification using RELION 2.0[13]. The particles from the best-aligned classes (106,581 particles) were then 3D auto-refined with D7 symmetry imposed using EMD-6287 as an initial model (low-passed filtered to 60 Å) to yield a ~7.4 Å resolution reconstruction (7.28 Å Nyquist). Particles were then re-centered using the refined particle offsets before being re-extracted unbinned (0.91 Å/pixel, 368 pixel box size) for 3D auto-refinement using a scaled output from the 4 x 4 binned refinement as an initial model. The refinement was continued using a soft-mask (3 pixel extension, 5 pixel soft cosine edge) generated from a volume contoured to display the full density. The final resolution was estimated as ~3.3 Å (gold-standard Fourier shell correlation (FSC)[14, 31, 32]) using phase-randomization to account for the convolution effects of a solvent mask on the FSC between the two independently refined half maps[32]. The refined particle coordinates were then used for local CTF estimation using gCTF[12] followed by re-extraction of particles using a 512 pixel box size to limit aliasing in the Fourier domain. Gold-standard 3D auto-refinement using the same soft mask yielded a ~3.1 Å reconstruction (gold-standard FSC) (Supplementary Figure 2). These particles were then subjected to 3D classification (k=4, tau fudge=25) without angular or translational searches using the same soft mask. However, further refinement of each individual class did not yield an improvement in nominal FSC-reported resolution. In addition, further filtering of the final particle stack using a cutoffs based on the height of the probability distributions at their maximum (MaxValueProbDistribution) did not result in an increase in nominal FSC-reported resolution. Finally, removal of all particles with an estimated defocus of greater than 1.5 μm yielded a reconstruction with the same reported resolution (~3.1 Å), indicating that particles illuminated at greater defoci did not significantly contribute high-resolution information (Supplementary Figure 3B).

In order to eliminate as many non optically-related discrepancies as possible between the stage movement and image shift collections, all the data were collected using sample grids prepared and frozen in parallel during back-to-back sessions on the Talos Arctica TEM with similar acquisition parameters (i.e. magnification, exposure rate, cumulative dose, etc.). Processing and refinement of the 20S proteasome data set collected using image shift was performed similarly as described for the 20S proteasome data set collected using stage position (Supplementary Figure 5).

810 movies (44 frames/movie) of rabbit muscle aldolase were acquired over 11 s with a exposure rate of 5.1 e^{-}/pixel/s, yielding a total dose of ~68 $e^{-}/Å^2$ (1.55 $e^{-}/Å^2$/frame), and a nominal defocus range from −0.8 μm to −1.4 μm. 2 × 2 Fourier-binned super-resolution images (0.91 Å /pixel) were motion correction and dose-weighted using the MotionCor2 program[10] using 5 x 5 tiled frames with a B-factor of 100 applied. Thon rings in the FFT of motion-corrected aldolase movies were visible to ~3 Å. Unweighted summed images were used for CTF determination using CTFFIND4[11]. Weighted sums were used for automated template-based particle picking with FindEM[30]. Only those micrographs with CC ≥90% and

with resolution estimates 5 Å or better at CC=50% (659 total) were used. 1,009,341 particles were extracted from these micrographs and binned 4 x 4 (3.64 Å/pixel, 92 pixel box size). Reference-free 2D classification in RELION 2.0[13] was then used to sort out non-particles and poor-quality picks in the data. A total of 652,869 particles corresponding to 2D class averages that displayed strong secondary-structural elements were selected for homogenous ab-initio model generation using cryoSPARC[33] to eliminate potential model bias. The generated volume was low-pass filtered to 30 Å and used as an initial model for 3D auto-refinement in RELION with D2 symmetry applied. The refined particle coordinates were then used for local CTF estimation using gCTF[12] followed by re-extraction of particles binned 2 x 2 (1.82 Å/pixel). Due to the close proximity of neighboring particles, any re-centered particle within a 32 pixel range of another was considered a duplicate and subsequently removed. The resulting stack, consisting of 606,278 particles, was subjected to 3D auto-refinement using the 4 x 4 binned map obtained from the previous refinement as an initial model. The refinement was continued using a soft mask (5 pixel extension, 10 pixel soft cosine edge) generated from a volume contoured to display the full density. The final resolution was estimated as ~3.6 Å (Nyquist=3.64 Å, gold-standard FSC[14, 31]) using phase-randomization to account for the convolution effects of a solvent mask on the FSC between the two independently refined half maps[32]. These particles were then subjected to 3D classification (k=6, tau fudge=8) without angular or translational searches using the same soft mask. Particles contributing to the classes that possessed the best resolved side-chain and backbone densities were re-centered, re-extracted, and cleaned of duplicates (83,910 particles, 0.91 Å/pixel, 368 pixel box size). These particles were then 3D auto-refined using a soft mask. The final resolution was estimated as ~2.6 Å (gold-standard FSC) (Supplementary Figure 1).

Local resolutions for all reconstructions were calculated using the “bloc_res” function in BSOFT[34].

Model building and refinement

For each of the final reconstructions, an initial model was subjected to a multi-model pipeline using methodologies similar to those described previously[35]. Briefly, for the 20S proteasome reconstructions, PDB ID:1YAR was stripped of all ligands (i.e. PA26 and waters) and all alternative conformations, all occupancies were set to unity, a single B-factor value was set for all atoms, and all Ramachandran and geometric outliers were corrected. For aldolase, PDB ID: 6ALD was stripped of all cofactors and water molecules, with all occupancies set to zero and all Ramachandran and geometric outliers corrected. Initial docking of PDB ID: 6ALD into the density revealed additional density beyond the Cβ of alanine 146. Analysis of the UniProt[36] metadata associated with PDB ID: 6ALD indicated this amino acid should be a lysine. Thus, lys146 was corrected in each chain prior to refinement. These initial models were then refined into the EM density using the imposed symmetry and estimated resolution while adjusting the Rosetta weighting and scoring functions according to the estimated map resolution.

Each of the 100 Rosetta-generated models[37] were ranked based on the number of Ramachandran outliers (%, lower better), geometry violations (%, lower better), Rosetta

aggregate score (value, lower better), and MolProbity clashscore[38] (value, lower better). The top 10 structures that scored the best across all categories were selected for real-space refinement using the Phenix refinement package[39]. Model–model agreement statistics were calculated using a previously described approach[35].

Supplementary Material

Refer to Web version on PubMed Central for supplementary material.

Acknowledgments

We thank Jean-Christophe Ducom at The Scripps Research Institute High Performance Computing for computational support, Bill Anderson at The Scripps Research Institute electron microscopy facility for microscope support, and Matthijn Vos for advice and discussion regarding microscope alignments. We are grateful to Yifan Cheng and Zanlin Yu for kindly providing the 20S sample used in this study. M.A.H. is supported by a Helen Hay Whitney Foundation postdoctoral fellowship. G.C.L. is supported as a Searle Scholar, a Pew Scholar, and by the National Institutes of Health (NIH) DP2EB020402. Computational analyses of EM data were performed using shared instrumentation funded by NIH S10OD021634.

References

1. Merk A, et al. Breaking Cryo-EM Resolution Barriers to Facilitate Drug Discovery. Cell. 2016; 165:1698–1707. [PubMed: 27238019]
2. Danev R, Tegunov D, Baumeister W. Using the Volta phase plate with defocus for cryo-EM single particle analysis. Elife. 2017; 6
3. Henderson R. The potential and limitations of neutrons, electrons and X-rays for atomic resolution microscopy of unstained biological molecules. Q Rev Biophys. 1995; 28:171–193. [PubMed: 7568675]
4. Campbell MG, et al. Near-atomic resolution reconstructions using a mid-range electron microscope operated at 200 kV. J Struct Biol. 2014; 188:183–187. [PubMed: 25278130]
5. Li X, et al. Near-Atomic Resolution Structure Determination of a Cypovirus Capsid and Polymerase Complex Using Cryo-EM at 200kV. J Mol Biol. 2017; 429:79–87. [PubMed: 27914893]
6. Glaeser RM, Typke D, Tiemeijer PC, Pulokas J, Cheng A. Precise beam-tilt alignment and collimation are required to minimize the phase error associated with coma in high-resolution cryo-EM. J Struct Biol. 2011; 174:1–10. [PubMed: 21182964]
7. Suloway C, et al. Automated molecular microscopy: the new Leginon system. J Struct Biol. 2005; 151:41–60. [PubMed: 15890530]
8. Lander GC, et al. Appion: an integrated, database-driven pipeline to facilitate EM image processing. J Struct Biol. 2009; 166:95–102. [PubMed: 19263523]
9. Russo CJ, Passmore LA. Electron microscopy: Ultrastable gold substrates for electron cryomicroscopy. Science. 2014; 346:1377–1380. [PubMed: 25504723]
10. Zheng SQ, et al. MotionCor2: anisotropic correction of beam-induced motion for improved cryo-electron microscopy. Nat Methods. 2017; 14:331–332. [PubMed: 28250466]
11. Rohou A, Grigorieff N. CTFFIND4: Fast and accurate defocus estimation from electron micrographs. J Struct Biol. 2015; 192:216–221. [PubMed: 26278980]
12. Zhang K. Gctf: Real-time CTF determination and correction. J Struct Biol. 2016; 193:1–12. [PubMed: 26592709]
13. Kimanius D, Forsberg BO, Scheres SH, Lindahl E. Accelerated cryo-EM structure determination with parallelisation using GPUs in RELION-2. Elife. 2016; 5
14. Henderson R, et al. Outcome of the first electron microscopy validation task force meeting. Structure. 2012; 20:205–214. [PubMed: 22325770]
15. Campbell MG, Veesler D, Cheng A, Potter CS, Carragher B. 2.8 A resolution reconstruction of the Thermoplasma acidophilum 20S proteasome using cryo-electron microscopy. Elife. 2015; 4

16. Egerton RF. Choice of operating voltage for a transmission electron microscope. Ultramicroscopy. 2014; 145:85–93. [PubMed: 24679438]
17. Campbell MG, et al. Movies of ice-embedded particles enhance resolution in electron cryo-microscopy. Structure. 2012; 20:1823–1828. [PubMed: 23022349]
18. Li X, et al. Electron counting and beam-induced motion correction enable near-atomic-resolution single-particle cryo-EM. Nat Methods. 2013; 10:584–590. [PubMed: 23644547]
19. Rubinstein JL, Brubaker MA. Alignment of cryo-EM movies of individual particles by optimization of image translations. J Struct Biol. 2015; 192:188–195. [PubMed: 26296328]
20. Grant T, Grigorieff N. Measuring the optimal exposure for single particle cryo-EM using a 2.6 A reconstruction of rotavirus VP6. Elife. 2015; 4:e06980. [PubMed: 26023829]
21. Scheres SH. Beam-induced motion correction for sub-megadalton cryo-EM particles. Elife. 2014; 3:e03665. [PubMed: 25122622]
22. Cheng Y, Grigorieff N, Penczek PA, Walz T. A primer to single-particle cryo-electron microscopy. Cell. 2015; 161:438–449. [PubMed: 25910204]
23. Khoshouei M, Radjainia M, Baumeister W, Danev R. Cryo-EM structure of haemoglobin at 3.2 A determined with the Volta phase plate. Nat Commun. 2017; 8:16099. [PubMed: 28665412]
24. Barad BA, et al. EMRinger: side chain-directed model and map validation for 3D cryo-electron microscopy. Nat Methods. 2015; 12:943–946. [PubMed: 26280328]
25. Dubochet J, et al. Cryo-electron microscopy of vitrified specimens. Q Rev Biophys. 1988; 21:129–228. [PubMed: 3043536]
26. Grassucci RA, Taylor D, Frank J. Visualization of macromolecular complexes using cryo-electron microscopy with FEI Tecnai transmission electron microscopes. Nat Protoc. 2008; 3:330–339. [PubMed: 18274535]
27. Asadabad, MA., Eskandari, MJ. Modern Electron Microscopy in Physical and Life Sciences. Janacek, M., Kral, R., editors. InTech; 2016.
28. Voss NR, Yoshioka CK, Radermacher M, Potter CS, Carragher B. DoG Picker and TiltPicker: software tools to facilitate particle selection in single particle electron microscopy. J Struct Biol. 2009; 166:205–213. [PubMed: 19374019]
29. Ogura T, Iwasaki K, Sato C. Topology representing network enables highly accurate classification of protein images taken by cryo electron-microscope without masking. J Struct Biol. 2003; 143:185–200. [PubMed: 14572474]
30. Roseman AM. FindEM--a fast, efficient program for automatic selection of particles from electron micrographs. J Struct Biol. 2004; 145:91–99. [PubMed: 15065677]
31. Scheres SH, Chen S. Prevention of overfitting in cryo-EM structure determination. Nat Methods. 2012; 9:853–854. [PubMed: 22842542]
32. Chen S, et al. High-resolution noise substitution to measure overfitting and validate resolution in 3D structure determination by single particle electron cryomicroscopy. Ultramicroscopy. 2013; 135:24–35. [PubMed: 23872039]
33. Punjani A, Rubinstein JL, Fleet DJ, Brubaker MA. cryoSPARC: algorithms for rapid unsupervised cryo-EM structure determination. Nat Methods. 2017; 14:290–296. [PubMed: 28165473]
34. Cardone G, Heymann JB, Steven AC. One number does not fit all: mapping local variations in resolution in cryo-EM reconstructions. J Struct Biol. 2013; 184:226–236. [PubMed: 23954653]
35. Herzik MA, Fraser JS, Lander GC. A multi-model approach to assessing local and global cryo-EM map quality. bioRxiv. 2017
36. Apweiler R, et al. UniProt: the Universal Protein knowledgebase. Nucleic Acids Res. 2004; 32:D115–119. [PubMed: 14681372]
37. Wang RY, et al. Automated structure refinement of macromolecular assemblies from cryo-EM maps using Rosetta. Elife. 2016; 5
38. Chen VB, et al. MolProbity: all-atom structure validation for macromolecular crystallography. Acta Crystallogr D Biol Crystallogr. 2010; 66:12–21. [PubMed: 20057044]
39. Adams PD, et al. PHENIX: a comprehensive Python-based system for macromolecular structure solution. Acta Crystallogr D Biol Crystallogr. 2010; 66:213–221. [PubMed: 20124702]

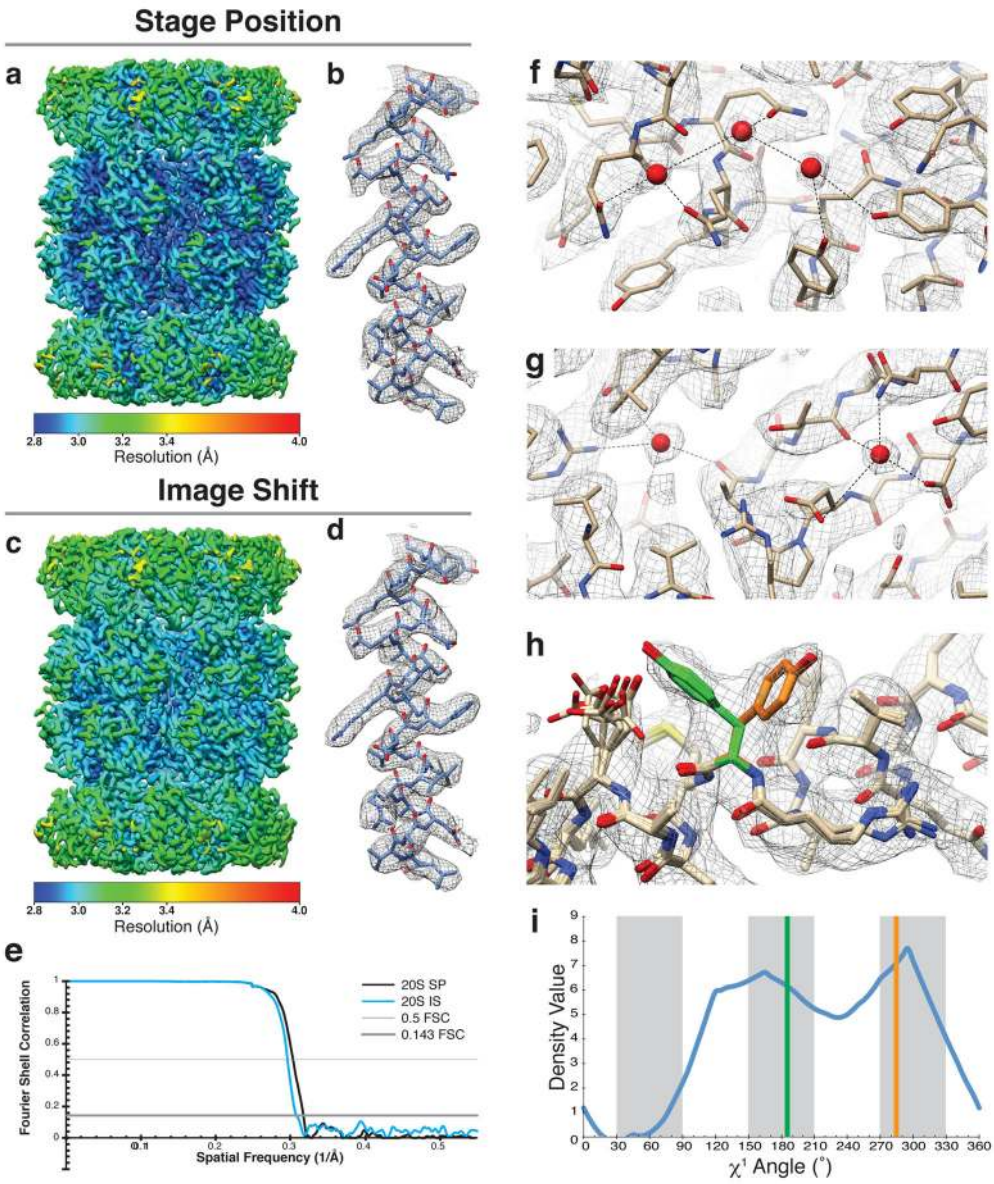

Figure 1. Cryo-EM reconstructions of the 20S proteasome at ~3.1 Å resolution

Local resolution estimates of the final *T. acidophilum* 20S proteasome reconstructions determined using either stage position (**a**) or image shift (**c**) navigation to exposure targets. An α-helix from the β-subunit (shown in stick representation) from each reconstruction with corresponding EM density (gray mesh, zoned 2 Å within atoms) exhibit clearly resolved side-chain density (**b** and **d**). (**e**) Gold-standard Fourier shell correlation curves indicate a final resolution of ~3.1 Å for the stage position dataset (black line) and ~3.3 Å for the image shift dataset (blue line). (**f** and **g**) The ~3 Å 20S EM density (gray mesh) is of sufficiently high resolution to observe ordered water molecules (shown as red spheres). Hydrogen bonds to the water molecules are shown as black dotted lines. (**h**) The EM density clearly shows that Tyr58 of the β-subunit adopts two alternative rotameric positions. The top 10 models refined against the density distribute into these rotameric positions, colored either orange

(60%) or green (40%). (**i**) EMRinger[24] analysis of the EM density corresponding to Tyr58 (blue line) confirms that the alternative conformations lie at ideal rotameric positions (thick gray bars). The refined χ^1 angles for Tyr58 are shown as vertical lines and colored according to panel C (conformation 1 is colored orange and conformation 2 is colored green).

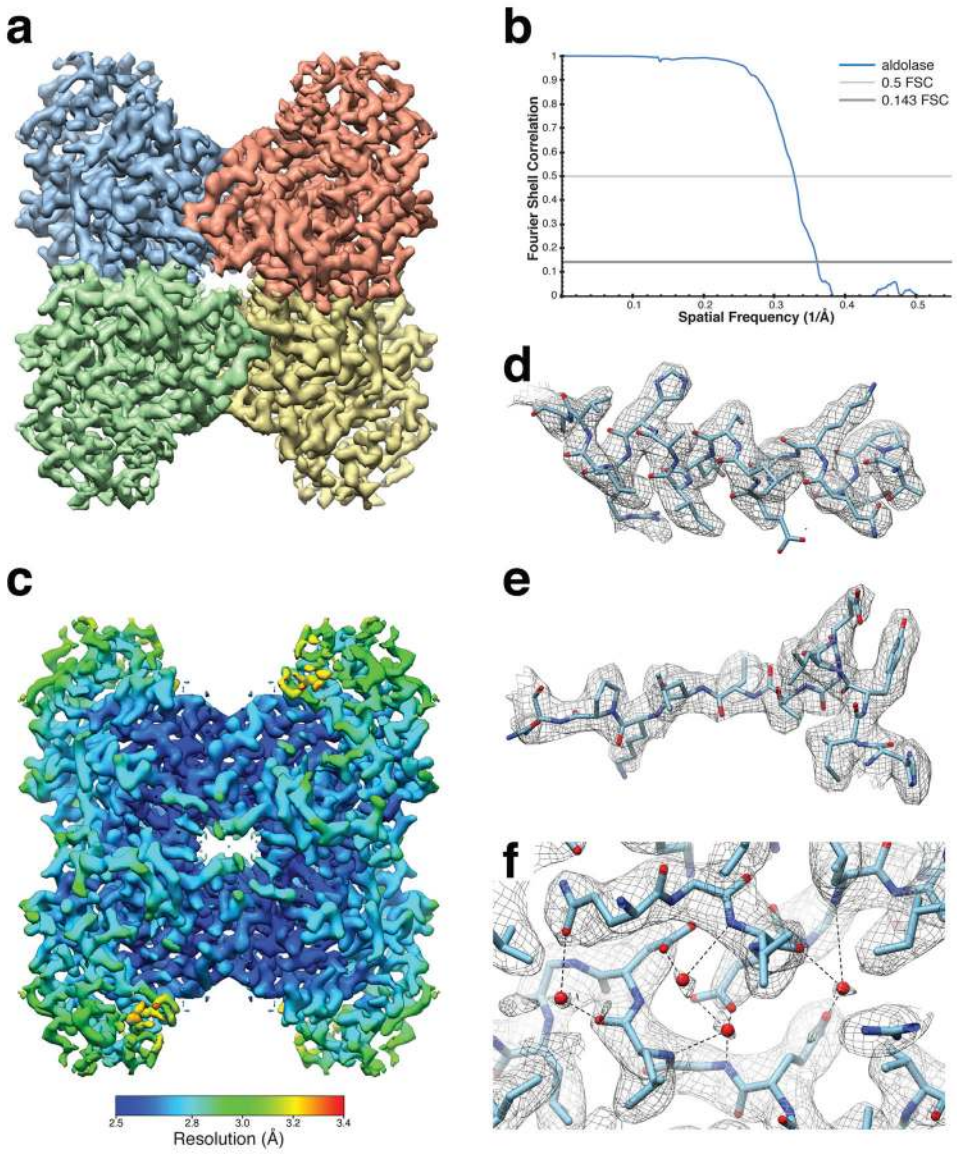

Figure 2. Structure of aldolase at ~2.6 Å resolution

(a) The ~2.6 Å resolution aldolase EM density (D2 symmetric) segmented based on protomer organization. **(b)** The gold-standard Fourier shell correlation curve indicates a final resolution of ~2.6 Å at 0.143 FSC. **(c)** The local resolution estimate of the final aldolase reconstruction reveals that most of the molecule is resolved to better than 2.8 Å, with the core of the molecule resolved to ~2.5 Å. **(d and e)** Representative regions of the aldolase EM density (gray mesh, zoned 2 Å within atoms) indicate the map is of sufficient quality to unambiguously assign side-chain conformations as well as **(f)** the placement of putative ordered water molecules.